J. Fluid Mech. (2008), *vol.* 601, *pp.* 407–424.
doi:10.1017/S0022112008000633 Printed in the United Kingdom

Energy amplification in channel flows of viscoelastic fluids

NAZISH HODA[1], MIHAILO R. JOVANOVIĆ[2] AND SATISH KUMAR[1]

[1]Department of Chemical Engineering and Materials Science, University of Minnesota, Minneapolis, MN 55455, USA

[2]Department of Electrical and Computer Engineering, University of Minnesota, Minneapolis, MN 55455, USA

(Received 24 October 2007 and in revised form 23 January 2008)

Energy amplification in channel flows of Oldroyd-B fluids is studied from an input–output point of view by analysing the ensemble-average energy density associated with the velocity field of the linearized governing equations. The inputs consist of spatially distributed and temporally varying body forces that are harmonic in the streamwise and spanwise directions and stochastic in the wall-normal direction and in time. Such inputs enable the use of powerful tools from linear systems theory that have recently been applied to analyse Newtonian fluid flows. It is found that the energy density increases with a decrease in viscosity ratio (ratio of solvent viscosity to total viscosity) and an increase in Reynolds number and elasticity number. In most of the cases, streamwise-constant perturbations are most amplified and the location of maximum energy density shifts to higher spanwise wavenumbers with an increase in Reynolds number and elasticity number and a decrease in viscosity ratio. For similar parameter values, the maximum in the energy density occurs at a higher spanwise wavenumber for Poiseuille flow, whereas the maximum energy density achieves larger maxima for Couette flow. At low Reynolds numbers, the energy density decreases monotonically when the elasticity number is sufficiently small, but shows a maximum when the elasticity number becomes sufficiently large, suggesting that elasticity can amplify disturbances even when inertial effects are weak.

1. Introduction

The inception and evolution of instabilities in viscoelastic fluid flows is an active area of research owing to the rich physical interactions present in and the enormous practical importance of such flows. Even for the seemingly simple cases of plane Couette and Poiseuille flows, understanding of the conditions under which instability occurs remains far less complete relative to that of Newtonian fluids (Morozov & Saarloos 2005). For plane Couette and Poiseuille flows of Newtonian fluids, it is now widely recognized that standard linear stability analysis can be misleading owing to the non-normal nature of the dynamical generator in the linear stability problem (Trefethen *et al.* 1993; Grossmann 2000; Schmid & Henningson 2001; Schmid 2007). Linear dynamical systems with non-normal generators can have solutions that grow substantially at short times, even though they decay at long times. This so-called transient growth would generally be overlooked in standard linear stability analysis (which typically focuses on only the least stable eigenvalues), and could put the system into a regime where nonlinear interactions are no longer negligible. The same issue

will arise for viscoelastic fluids, making it important to investigate transient growth phenomena in these flows as well.

Closely related to the issue of transient growth is the question of how sensitive the linearized equations are to external disturbances, for such disturbances may produce the initial conditions that lead to transient growth (Farrell & Ioannou 1993; Bamieh & Dahleh 2001; Schmid 2007). In a recent paper, Jovanović & Bamieh (2005) applied powerful tools from linear systems theory to study the effect of external disturbances on plane Couette and Poiseuille flows of Newtonian fluids. To the linearized Navier–Stokes equations, they added external disturbances in the form of spatially distributed and temporally varying body forces which were harmonic in the streamwise and spanwise directions and stochastic in the wall-normal direction and in time. The equations were then cast into 'state-space' form, in which the body forces are an input and the velocity field is an output, with the two being related through a transfer function operator. For inputs of the type considered, methods exist for calculating the ensemble-average energy density associated with the velocity field, and these were applied to characterize the amplification of disturbances for a wide range of streamwise and spanwise wavenumbers. In general, it was found that external disturbances can be considerably amplified, with the most amplified disturbances being those elongated in the streamwise direction (i.e. streamwise-constant perturbations). In addition, Jovanović & Bamieh (2005) were able to ascertain the extent to which individual components of the input vector affect individual components of the output vector.

The large amplification of external disturbances could be a route through which the initial conditions needed for transient growth are produced (Farrell & Ioannou 1993; Bamieh & Dahleh 2001; Jovanović & Bamieh 2005). In addition, the large amplification itself could trigger nonlinear effects, thereby providing a potential route by which a flow could become unstable to initially small-amplitude disturbances. It is worthwhile to note that although the external disturbances take the form of body forces, they can also be interpreted more generally as representing uncertainty in the mathematical model for the flow system (Bamieh & Dahleh 2001; Jovanović & Bamieh 2005; Schmid 2007). Such uncertainties may arise in the base flow, boundary conditions (e.g. wall roughness, non-parallel walls), and constitutive laws, or from the neglect of certain effects (e.g. nonlinearities, free-stream turbulence).

Numerous investigators have applied standard linear stability analysis to plane Couette and Poiseuille flows of viscoelastic fluids. The most basic constitutive equations for viscoelastic fluids are the upper-convected Maxwell (UCM) model and the Oldroyd-B model. The latter model can be derived from kinetic theory by considering a dilute suspension of Hookean dumbbells (which represent polymer molecules) in a Newtonian solvent, and the former model is obtained in the limit of the solvent contribution to the fluid viscosity being much smaller than that of the polymer (Bird *et al.* 1987; Larson 1999). When inertial effects are absent, plane Couette flow of UCM and Oldroyd-B fluids is stable (Gorodtsov & Leonov 1967; Wilson, Renardy & Renardy 1999), and no instabilities have been found at finite Reynolds number (Renardy & Renardy 1986; Kumar & Shankar 2005). In the Newtonian case, stability is also predicted at all Reynolds numbers (Romanov 1973). For plane Poiseuille flow, no instabilities are present under creeping-flow conditions for either Newtonian, UCM or Oldroyd-B fluids (Ho & Denn 1977; Sureshkumar & Beris 1995). When inertial effects are present, Newtonian fluids can become unstable above a critical Reynolds number (Orszag 1971). For UCM and Oldroyd-B fluids, the critical Reynolds number decreases, reaches a minimum, and then begins increasing

as the elasticity number (ratio of elastic to inertial forces) increases (Ho & Denn 1977; Sureshkumar & Beris 1995). Increasing the relative importance of the solvent viscosity has a stabilizing effect. Thus, for plane Poiseuille flow, elasticity is initially destabilizing before becoming stabilizing.

Studies of transient growth phenomena in viscoelastic fluids have also been carried out. Sureshkumar *et al.* (1999) performed two-dimensional time-dependent simulations of creeping plane Couette flow of Oldroyd-B fluids using both the linearized and fully nonlinear equations. They found that in each case, disturbances decay at long times but grow at short times, with higher levels of elasticity tending to enhance the transient growth. Atalik & Keunings (2002) reported the results of two-dimensional time-dependent simulations of plane Couette and Poiseuille flows of Oldroyd-B fluids using the fully nonlinear equations. They observed that for Poiseuille flow, disturbances of sufficiently large amplitude can grow, leading to a time-periodic flow. When inertial forces dominate elastic forces, the time-periodic states occur above a critical Reynolds number which decreases and then increases as the elasticity number increases. Increasing the contribution of the polymer viscosity to the total viscosity also decreases the critical Reynolds number. When elastic forces dominate inertial forces, time-periodic states occur if the elasticity number is sufficiently large and the solvent contribution to the viscosity is below a critical value. In contrast, disturbances in Couette flow were always found to decay in an oscillatory manner. Kupferman (2005) found new eigenfunctions of the two-dimensional linearized equations for plane Couette flow of an Oldroyd-B fluid. Pseudo-spectral analysis was then applied and revealed that these eigenfunctions exhibit transient growth. Doering, Eckhardt & Schumacher (2006) demonstrated that at finite Reynolds numbers it is not possible to exhibit monotonic decay of fluctuations in viscoelastic fluids. This was done by providing several examples of solutions to the governing equations for plane Couette flow of an Oldroyd-B fluid that show transient growth. In these examples, the perturbations to the base state are two-dimensional, and transient amplification requires the fluid elasticity to be sufficiently large. Finally, we note that recent weakly nonlinear analyses have predicted that plane Couette and Poiseuille flows of viscoelastic fluids are unstable to finite-amplitude perturbations even though standard linear stability analysis predicts that they are stable to small-amplitude perturbations (Meulenbroek *et al.* 2004; Morozov & Saarloos 2005). In this case, the nonlinearities that lead to the finite-amplitude instability could be triggered if the linearized equations allow perturbations to the flow to grow at short times.

In this paper, we extend the work of Jovanović & Bamieh (2005) to viscoelastic fluids. We use the Oldroyd-B model and explore the effects of the elasticity number and viscosity ratio on energy amplification over a range of Reynolds numbers. In § 2, we formulate the problem and describe the analysis method. A parametric study of the ensemble-average energy density associated with the velocity field is given in § 3; we find that, as with Newtonian fluids, external disturbances can be considerably amplified. Since streamwise-constant perturbations are found to be the most amplified in viscoelastic (as well as Newtonian) fluids, we undertake in § 4 a detailed parametric study for this case. Finally, we conclude and summarize the important findings in § 5.

2. Problem formulation and analysis method

In this section, we describe how the governing equations can be written in a form amenable to input–output analysis. We also introduce the notion of ensemble-average energy density, and briefly discuss a numerical technique for computing this quantity.

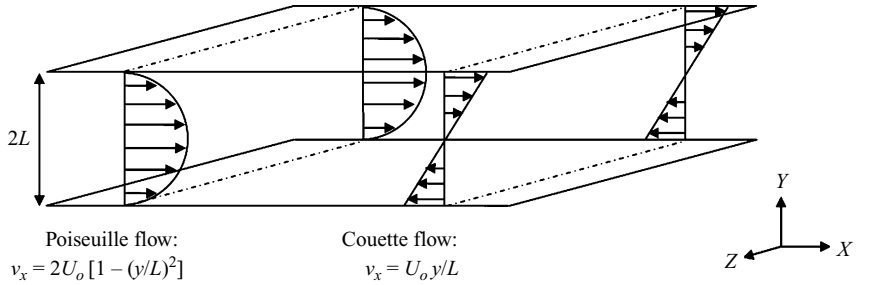

FIGURE 1. Schematic of the channel-flow geometry.

2.1. *Governing equations and geometry*

Figure 1 shows a schematic of the channel-flow geometry. For Couette flow, the top plate moves in the positive x-direction and the bottom plate moves in the negative x-direction, each with speed U_o. For Poiseuille flow, $2U_o$ is the centreline velocity. The height of the channel is $2L$, the fluid has relaxation time λ, and the polymer and solvent viscosities are η_p and η_s, respectively. The dimensionless momentum conservation, mass conservation, and constitutive equations are

$$\partial_t \boldsymbol{V} = -\boldsymbol{V}\cdot\nabla\boldsymbol{V} + \frac{1}{Re}(-\nabla P + \beta\nabla^2\boldsymbol{V} + (1-\beta)\nabla\cdot\boldsymbol{T}), \tag{2.1a}$$

$$0 = \nabla\cdot\boldsymbol{V}, \tag{2.1b}$$

$$\partial_t \boldsymbol{T} = \frac{1}{Wi}(\nabla\boldsymbol{V} + (\nabla\boldsymbol{V})^T) - \boldsymbol{V}\cdot\nabla\boldsymbol{T} + \boldsymbol{T}\cdot\nabla\boldsymbol{V} + (\boldsymbol{T}\cdot\nabla\boldsymbol{V})^T - \frac{\boldsymbol{T}}{Wi}, \tag{2.1c}$$

where $\boldsymbol{V} = [U\ V\ W]^T$ is the velocity vector, P is the pressure, $\boldsymbol{T}$ is the polymeric contribution to the stress tensor, $Re = \rho U_o L/(\eta_s + \eta_p)$ is the Reynolds number, and $\beta = \eta_s/(\eta_s + \eta_p)$ is the ratio of the solvent viscosity to the total viscosity. The Weissenberg number Wi, which is the ratio of the fluid relaxation time to the characteristic flow time, is given by $Wi = \lambda U_o/L$. The above equations have been non-dimensionalized by scaling length with L, velocity with U_o, polymer stresses with $\eta_p U_o/L$, time with L/U_o, and pressure with $(\eta_s + \eta_p)U_o/L$. We note that Wi/Re is known as the elasticity number, μ, which represents the ratio of the fluid relaxation time to the characteristic time for vorticity diffusion; this quantity provides a measure of the strength of elastic forces relative to inertial forces.

Equations (2.1) are linearized by decomposing the flow variables into contributions from the base state and fluctuations. Keeping terms only to first order in the fluctuations yields:

$$\partial_t \boldsymbol{v} = -\boldsymbol{v}\cdot\nabla\overline{\boldsymbol{v}} - \overline{\boldsymbol{v}}\cdot\nabla\boldsymbol{v} + \frac{1}{Re}(-\nabla p + \beta\nabla^2\boldsymbol{v} + (1-\beta)\nabla\cdot\boldsymbol{\tau}) + \boldsymbol{d},$$

$$0 = \nabla\cdot\boldsymbol{v},$$

$$\partial_t \boldsymbol{\tau} = \frac{1}{Wi}(\nabla\boldsymbol{v} + (\nabla\boldsymbol{v})^T) - \boldsymbol{v}\cdot\nabla\overline{\boldsymbol{\tau}} - \overline{\boldsymbol{v}}\cdot\nabla\boldsymbol{\tau} + \boldsymbol{\tau}\cdot\nabla\overline{\boldsymbol{v}} + \overline{\boldsymbol{\tau}}\cdot\nabla\boldsymbol{v} + (\overline{\boldsymbol{\tau}}\cdot\nabla\boldsymbol{v})^T + (\boldsymbol{\tau}\cdot\nabla\overline{\boldsymbol{v}})^T - \frac{\boldsymbol{\tau}}{Wi},$$

where variables with an overbar are base-state variables, $\boldsymbol{v} = [u\ v\ w]^T$ is the velocity fluctuation vector, p is the pressure fluctuation, and $\boldsymbol{\tau}$ is the polymer stress fluctuation. To the linearized equations we have added a spatially distributed and temporally varying body force, $\boldsymbol{d} = [d_1\ d_2\ d_3]^T$, where d_1, d_2, and d_3 are the body forces in the

streamwise (x), wall-normal (y), and spanwise (z) directions, respectively. These body forces serve as inputs into the linearized system of equations, and we wish to study their effect on the velocity field.

The unidirectional base flows are found by application of the no-slip and no-penetration boundary conditions. In Couette flow, we obtain

$$\overline{\boldsymbol{v}} = [\ \overline{U}\ \ \overline{V}\ \ \overline{W}]^T = [\ y\ \ 0\ \ 0\ ]^T, \quad \overline{\boldsymbol{\tau}} = \begin{bmatrix} 2Wi & 1 & 0 \\ 1 & 0 & 0 \\ 0 & 0 & 0 \end{bmatrix},$$

and in Poiseuille flow we have

$$\overline{\boldsymbol{v}} = [\overline{U}\ \ \overline{V}\ \ \overline{W}]^T = [1 - y^2\ 0\ 0]^T, \quad \overline{\boldsymbol{\tau}} = \begin{bmatrix} 8y^2Wi & -2y & 0 \\ -2y & 0 & 0 \\ 0 & 0 & 0 \end{bmatrix}.$$

2.2. *Description of the input–output analysis*

The input–output analysis is facilitated by writing the governing equations in terms of wall-normal velocity (v) and vorticity (ω_y) variables (Schmid & Henningson 2001). In addition, since the base flow is constant in the streamwise and the spanwise directions, the Fourier transform is applied in these directions. (We use the same symbol for representing a variable and its Fourier transform.) This leads to the following representation:

$$\left.\begin{aligned} \partial_t \boldsymbol{\psi}(k_x, y, k_z, t) &= [\boldsymbol{A}(k_x, k_z)\boldsymbol{\psi}(k_x, k_z, t)](y) + [\overline{\boldsymbol{B}}(k_x, k_z)\boldsymbol{d}(k_x, k_z, t)](y), \\ \boldsymbol{v}(k_x, y, k_z, t) &= [\boldsymbol{C}(k_x, k_z)\boldsymbol{\psi}_1(k_x, k_z, t)](y), \end{aligned}\right\} \tag{2.2}$$

where k_x and k_z are the streamwise and spanwise wavenumbers, $\boldsymbol{\psi} = [\boldsymbol{\psi}_1^T\ \ \boldsymbol{\psi}_2^T\ ]^T$, $\boldsymbol{\psi}_1 = [v\ \omega_y]^T$, and $\boldsymbol{\psi}_2 = [\tau_{xx}\ \tau_{yy}\ \tau_{zz}\ \tau_{xy}\ \tau_{xz}\ \tau_{yz}]^T$, with τ_{ij} denoting the components of $\boldsymbol{\tau}$. The operator $\boldsymbol{A}$ has the following form:

$$\boldsymbol{A} = \begin{bmatrix} \boldsymbol{A}_{11} & \boldsymbol{A}_{12} \\ \boldsymbol{A}_{21} & \boldsymbol{A}_{22} \end{bmatrix}, \tag{2.3}$$

where the operator blocks in (2.3) are defined in the Appendix. It should be noted that in Newtonian fluids, there is only one block, $\boldsymbol{A}_{11}$, and in the limit $\beta \to 1$, $\boldsymbol{A}_{11}$ in (2.3) simplifies to the dynamical generator in familiar Orr–Sommerfeld and Squire equations of Newtonian fluids. The operator $\boldsymbol{A}_{12}$ describes how polymer stresses enter into the equations governing the evolution of wall-normal velocity and vorticity. On the other hand, the operators $\boldsymbol{A}_{21}$ and $\boldsymbol{A}_{22}$ appear in the constitutive equation, where $\boldsymbol{A}_{21}$ acts on the wall-normal velocity/vorticity and $\boldsymbol{A}_{22}$ acts on the polymer stress. Furthermore, $\overline{\boldsymbol{B}}$ is an 8×3 matrix of operators, which we denote as $\overline{\boldsymbol{B}} = [\boldsymbol{B}^T\ \ \boldsymbol{O}^T]^T$, where $\boldsymbol{O}$ is a 6×3 null matrix. We note that operator $\boldsymbol{B}$ describes how forcing enters the Orr–Sommerfeld and Squire equations of viscoelastic channel flows, and operator $\boldsymbol{C}$ in (2.2) captures a kinematic relationship between the wall-normal velocity/vorticity vector $\boldsymbol{\psi}_1$ and velocity fluctuation vector $\boldsymbol{v}$. The definitions of these two operators are provided in the Appendix (see Jovanović & Bamieh (2005) for additional details).

System of equations (2.2) is referred to as a state-space representation in the control literature (Curtain & Zwart 1995), where $\boldsymbol{d}$ is the disturbance or input, $\boldsymbol{\psi}$ is the state of the system, and $\boldsymbol{v}$ is the system response or output. In the state-space formulation, the following boundary conditions are imposed on the wall-normal velocity and vorticity

variables:

$$v(k_x, \pm 1, k_z, t) = \partial_y v(k_x, \pm 1, k_z, t) = \omega_y(k_x, \pm 1, k_z, t) = 0. \tag{2.4}$$

These boundary conditions come from the no-slip and no-penetration requirements on the velocity field components. It is worth mentioning that no boundary conditions on the polymer stresses are required since in (2.2) there are no terms involving derivatives of these stresses with respect to y.

For disturbances harmonic in x and z and random (zero-mean white noise) in y and t, the energy amplification for a given k_x and k_z can be determined by calculating the H_2 norm, whose square is also known as the ensemble-average energy density (herein referred to as energy density) (Farrell & Ioannou 1993). The energy density of a stochastic velocity field is determined by

$$E(k_x, k_z) = \lim_{t\to\infty} \left(\frac{1}{8} \int_{-1}^{1} \mathscr{E}(\boldsymbol{v}^*(k_x, y, k_z, t)\boldsymbol{v}(k_x, y, k_z, t))\, \mathrm{d}y \right),$$

where asterisk denotes complex-conjugate transpose of vector $\boldsymbol{v}$, and $\mathscr{E}$ denotes ensemble averaging (McComb 1991), that is

$$\mathscr{E}(\boldsymbol{v}(\cdot, t)) = \lim_{T\to\infty} \frac{1}{T} \int_0^T \boldsymbol{v}(\cdot, t+\tau)\, \mathrm{d}\tau.$$

We note that the stochastic character of velocity field $\boldsymbol{v}$ arises due to the randomness of input field $\boldsymbol{d}$ (Farrell & Ioannou 1993).

The energy density can also be defined in terms of the frequency response operator, $H(k_x, k_z, \omega)$, where ω is a temporal frequency. For any triplet (k_x, k_z, ω), the frequency response is an operator (in the wall-normal direction) that maps the spatio-temporal Fourier transform of the forcing field to the spatio-temporal Fourier transform of the velocity field, i.e.

$$\boldsymbol{v}(k_x, y, k_z, \omega) = [H(k_x, k_z, \omega)\boldsymbol{d}(k_x, k_z, \omega)](y).$$

The energy density is then obtained by averaging over the wall-normal direction and time:

$$E(k_x, k_z) = \frac{1}{2\pi} \int_{-\infty}^{\infty} \mathrm{trace}(H(k_x, k_z, \omega)H^*(k_x, k_z, \omega))\, \mathrm{d}\omega,$$

where H^* denotes the adjoint of operator H. The averaging in y is obtained by computing the Hilbert–Schmidt norm of operator H, $\|H\|_{HS}^2 = \mathrm{trace}(HH^*)$, and averaging in time is obtained by integration over temporal frequencies.

It is essential to note that the energy density can be evaluated without doing an explicit temporal-frequency integration (Zhou, Doyle & Glover 1996); namely, this quantity is determined by

$$E(k_x, k_z) = \mathrm{trace}(\boldsymbol{X}_{11}(k_x, k_z)\boldsymbol{C}^*(k_x, k_z)\boldsymbol{C}(k_x, k_z)),$$

where $\boldsymbol{X}_{11}$ is the 11-block of operator $\boldsymbol{X}$, which is given by:

$$\boldsymbol{X} = \begin{bmatrix} \boldsymbol{X}_{11} & \boldsymbol{X}_{12} \\ \boldsymbol{X}_{12}^* & \boldsymbol{X}_{22} \end{bmatrix}.$$

The self-adjoint operator $\boldsymbol{X}$ is partitioned conformably with the elements of operator $\boldsymbol{A}$ and it can be determined by solving the following operator Lyapunov equation

(Farrell & Ioannou 1993; Bamieh & Dahleh 2001; Jovanović & Bamieh 2005):

$$\boldsymbol{A}(k_x, k_z)\boldsymbol{X}(k_x, k_z) + \boldsymbol{X}(k_x, k_z)\boldsymbol{A}^*(k_x, k_z) = -\overline{\boldsymbol{B}}(k_x, k_z)\overline{\boldsymbol{B}}^*(k_x, k_z).$$

The elements of $\boldsymbol{X}$ are related to correlation functions involving the elements of $\boldsymbol{\psi}$ (Bamieh & Dahleh 2001); namely, the steady-state covariance operator of $\boldsymbol{\psi}_i$ with itself is given by $\boldsymbol{X}_{ii}$, and the steady-state covariance operator of $\boldsymbol{\psi}_1$ with $\boldsymbol{\psi}_2$ is given by $\boldsymbol{X}_{12}$. We refer the reader to the Appendix for the definitions of the adjoints of operators $\boldsymbol{A}$, $\boldsymbol{B}$, and $\boldsymbol{C}$.

2.3. *Numerical method*

From the above Lyapunov equation, a system of eight operator-valued equations (in y) can be generated. These are discretized using a Chebyshev collocation technique so that all the variables are approximated by a set of Chebyshev polynomials that satisfy the boundary conditions (2.4) (Canuto *et al.* 1988). The matrix representation for all the operators can be obtained without numerical integration as there is a recursive relationship between the Chebyshev polynomials and their derivatives (Boyd 1989), which is implemented using a public-domain MATLAB subroutine (Weideman & Reddy 2000). This effectively replaces the eight operator-valued equations with $8N$ linear algebraic equations, where N denotes the number of collocation points. The algebraic Lyapunov equations are solved using the lyap subroutine in MATLAB. All the results presented in this study were checked for convergence by varying the number of collocation points. In most of the cases, between 30 to 50 collocation points were found to be sufficient to obtain accurate results. At the higher Reynolds numbers and elasticity numbers investigated, approximately 100 collocation points were needed since under these conditions there are larger gradients in the solution near the channel walls. The results were also verified by comparing with the known results in the Newtonian limit (Jovanović & Bamieh 2005). In all of the plots presented in § 3, 50×30 grid points were used in the (k_x, k_z)-space. The streamwise and spanwise wavenumbers are varied in a logarithmic scale between 10^{-4} and 3.02 (for k_x) and between 10^{-2} and 5 (for k_z).

3. Parametric behaviour of energy amplification

Here, we study the effect of viscosity ratio and elasticity number on the ensemble-average energy density. The energy density quantifies the aggregate effect of disturbances in all three spatial directions on all three velocity components.

We first examine the effect of viscosity ratio on the energy density. It should be noted that an Oldroyd-B fluid is equivalent to an UCM fluid for $\beta \to 0$ and a Newtonian fluid for $\beta \to 1$. Figure 2 shows the energy density for $Re = 1000$, $\mu = 10$, and $\beta = \{0.1, 0.5, 0.9\}$ in both Couette and Poiseuille flows. In all cases, the energy density peaks in a narrow region near $k_x \approx 0$, indicating the dominance of streamwise-elongated structures (Schmid & Henningson 2001). For $\mu = 10$, as β increases these peaks shift from $k_x = 0$ to small non-zero values of k_x, indicating the larger prominence of weakly oblique velocity perturbations. Furthermore, with an increase in β, significant energy amplification is observed for a wider range of k_x and the maximum in energy density shifts to smaller values of k_z, suggesting that the dominant flow structures become more spread in the z-direction. We also note that the maximum energy amplification decreases with an increase in β (i.e. as the Newtonian limit is approached). In both Couette and Poiseuille flows, there is an order-of-magnitude difference in the maximum energy density between $\beta = 0.1$ and $\beta = 0.5$, as well as for $\beta = 0.5$ and

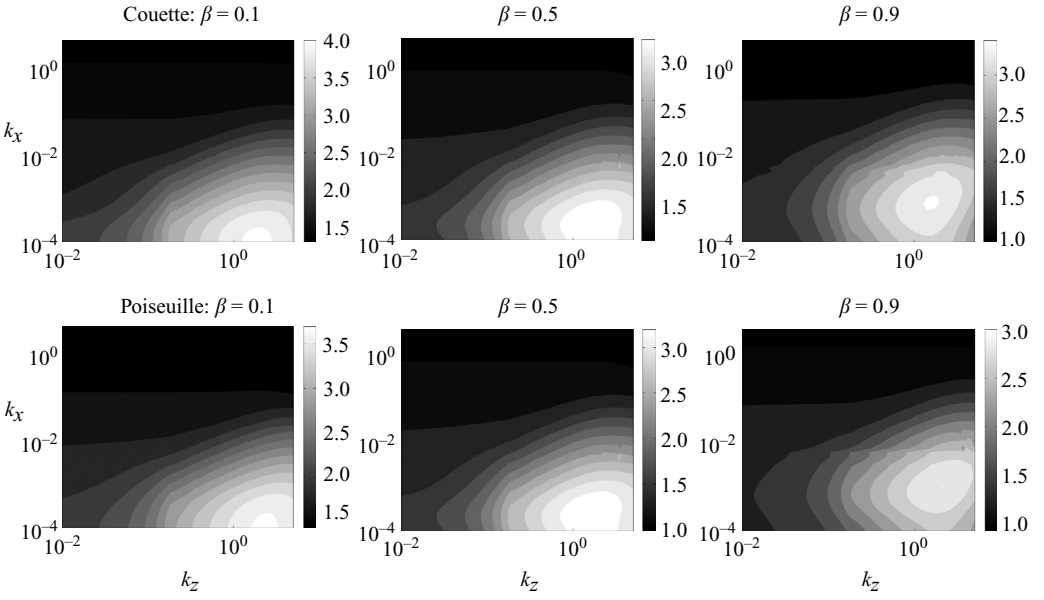

FIGURE 2. Ensemble-average energy density, $(1/2)\log_{10}(E(k_x, k_z))$, for $Re = 1000$ and $\mu = 10$ in both Couette and Poiseuille flows.

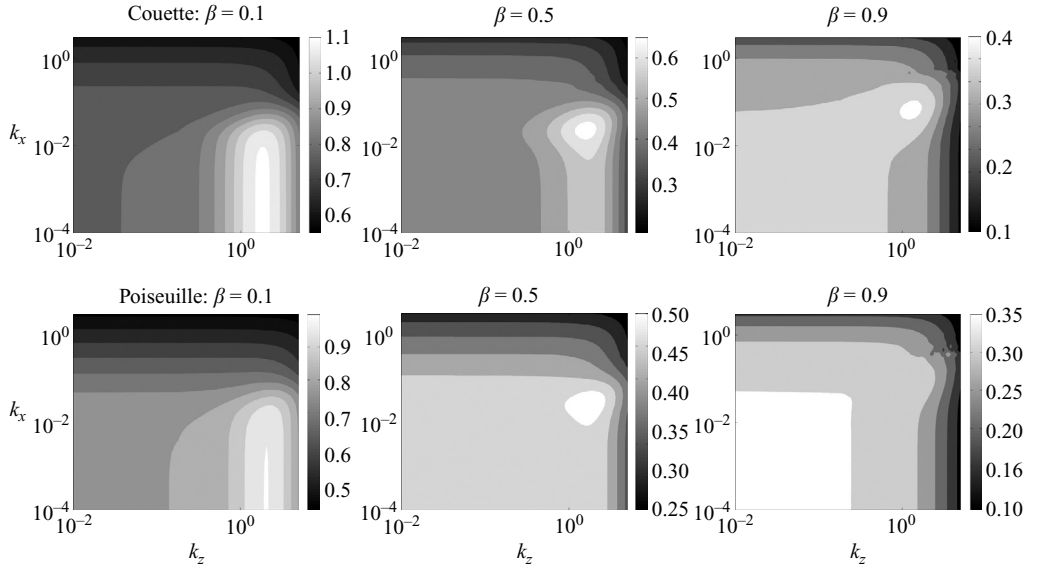

FIGURE 3. Ensemble-average energy density, $(1/2)\log_{10}(E(k_x, k_z))$, for $Re = 10$ and $\mu = 10$ in both Couette and Poiseuille flows.

$\beta = 0.9$. The maximum in energy density is located at a higher k_z for Poiseuille flow compared to Couette flow, but the maximum value of the energy density is smaller in this case.

Similar trends are observed at $Re = 10$, as shown in figure 3. Here, the maximum energy density is located at larger values of k_x than for $Re = 1000$, indicating the increasing importance of oblique perturbations ($k_x = O(1), k_z = O(1)$). In general,

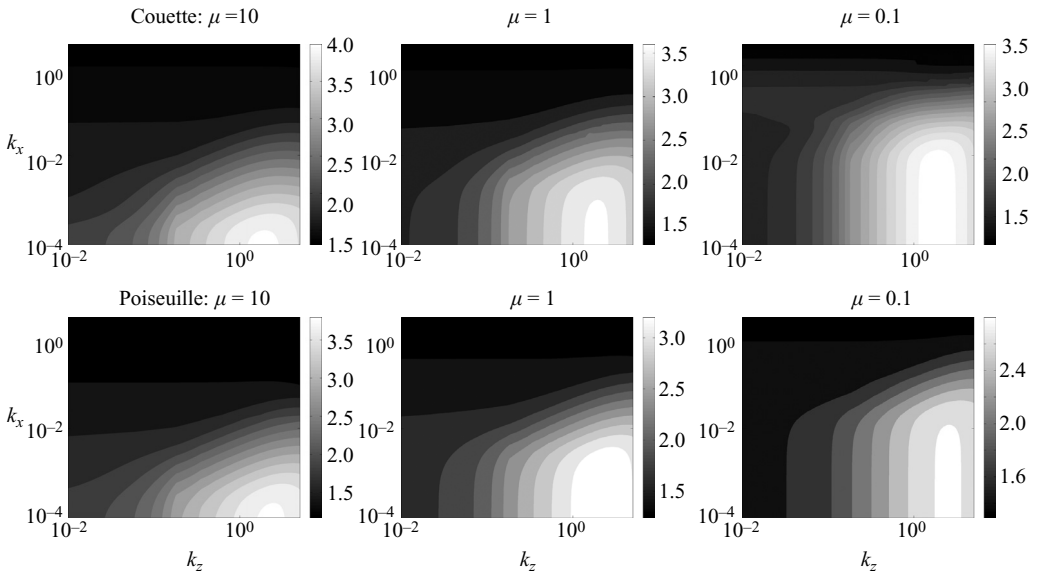

FIGURE 4. Ensemble-average energy density, $(1/2)\log_{10}(E(k_x, k_z))$, for $Re = 1000$ and $\beta = 0.1$ in both Couette and Poiseuille flows.

lowering Re leads to smaller energy amplification, broadens the range of (k_x, k_z) over which there is significant energy amplification, and leads to flow structures that have larger spanwise length scales (i.e. smaller values of k_z).

Figure 4 shows the energy density in both Couette and Poiseuille flow for $Re = 1000$, $\beta = 0.1$, and $\mu = \{0.1, 1, 10\}$. It is clear from the plots that the magnitude of the maximum energy density decreases with a decrease in μ and is smaller for Poiseuille flow than for Couette flow. For this particular set of parameters, the location of maximum energy amplification does not depend on μ (i.e. it takes place at $k_x = 0$, $k_z = O(1)$). Typically, the maximum shifts to smaller values of k_z with a decrease in μ, indicating that the dominant flow structures have larger length scales in the z-direction. Also, at smaller μ values, significant energy amplification is observed for a wider range of streamwise and spanwise wavenumbers.

The results of this section clearly illustrate that increasing the fluid elasticity through either the polymer contribution to the viscosity or the elasticity number enhances energy amplification. The disturbances that are most amplified tend to be streamwise-elongated, with elasticity acting to reduce their spanwise length scale.

4. Energy amplification of streamwise-constant perturbations

Since in most cases the streamwise-elongated perturbations experience the largest energy amplification, we focus here on the case where $k_x = 0$ and perform a detailed parametric study exploring the effects of Re, μ, and β.

4.1. *Effect of Re*

Figure 5 shows the dependence of the energy density on k_z for different Reynolds numbers in both Couette and Poiseuille flows. Although the plots are presented for a particular set of β and μ values, the trends are qualitatively similar for other values of β and μ. In both Couette and Poiseuille flows, the energy density

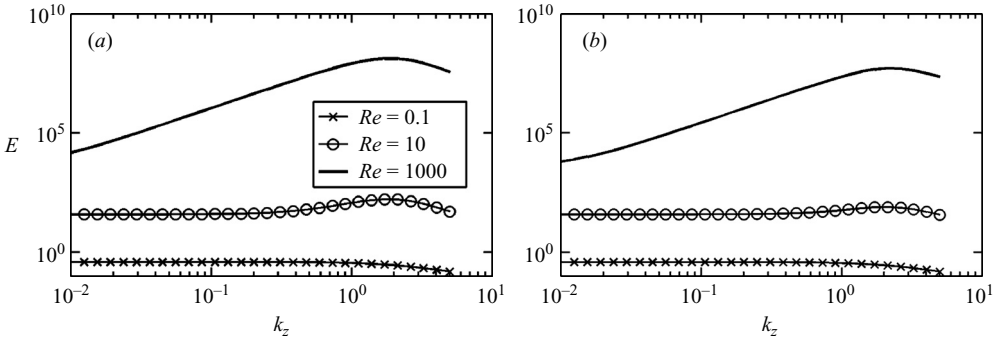

FIGURE 5. Variation of $E(k_z)$ with k_z for streamwise-constant perturbations at different Re for $\beta = 0.1$ and $\mu = 10$: (*a*) Couette flow; (*b*) Poiseuille flow.

monotonically decreases with an increase in k_z at very small values of Re. At higher Reynolds numbers, the energy density shows a maximum in k_z, indicating that the amplification is largest for non-zero spanwise wavenumber disturbances. In channel flows of Newtonian fluids, the energy amplification at $k_x = 0$ scales as $f(k_z)Re + g(k_z)Re^3$ (Bamieh & Dahleh 2001; Jovanović & Bamieh 2005), where the f and g functions are Re-independent. We have utilized frequency response analysis to establish a similar scaling law for viscoelastic fluids (Hoda, Jovanović & Kumar 2008); namely, the energy amplification of streamwise-constant channel flows of Oldroyd-B fluids is given by $q(k_z, \beta, \mu)Re + r(k_z, \beta, \mu)Re^3$ where functions q and r do not depend on the Reynolds number. For Newtonian fluids, vortex stretching (which is proportional to $\overline{U}'\partial_z v$) is responsible for the energy amplification (Landahl 1975; Butler & Farrell 1992). Jovanović & Bamieh (2005) showed analytically that the singular values of the frequency response operator scale as Re^2 only when the vortex stretching term is non-zero (otherwise the Re^2 term is absent and they scale as Re); it is this scaling that gives rise to Re^3 scaling of the energy density (Jovanović & Bamieh 2005). We have shown that even in the case of Oldroyd-B fluids, the vortex stretching term contributes to the Re^2-scaling of the singular values of the frequency response operator (Hoda *et al.* 2008). This demonstrates the importance of the vortex stretching mechanism (Landahl 1975) in viscoelastic fluids.

4.2. *Effect of* β

The variation in the energy density with k_z at different β and μ for $Re = 1000$ is shown in figure 6. The observation that the energy amplification increases as β decreases is consistent with observations of standard two-dimensional linear stability analysis. When comparing the stability characteristics of the Oldroyd-B and UCM models for plane Poiseuille flow, Sureshkumar & Beris (1995) found that the presence of non-zero solvent viscosity has a pronounced stabilizing effect on the flow.

The dependence of the energy density on β can be better understood by interrogating system (2.2). We identified three terms where the viscosity ratio appears as a prefactor. In the operator $\boldsymbol{A}_{11}$, defined in the Appendix, β is a prefactor to the term $\Delta^{-1}\Delta^2 v$, which is the viscous stress term, and the term $\Delta\eta$, which is the vorticity diffusion term. The viscosity ratio also appears as a prefactor, $(1-\beta)$, in the operator $\boldsymbol{A}_{12}$, defined in the Appendix. Here, we label the viscosity ratio in front of the viscous stress term and vorticity diffusion term as β_1 and β_2, respectively, and the prefactor

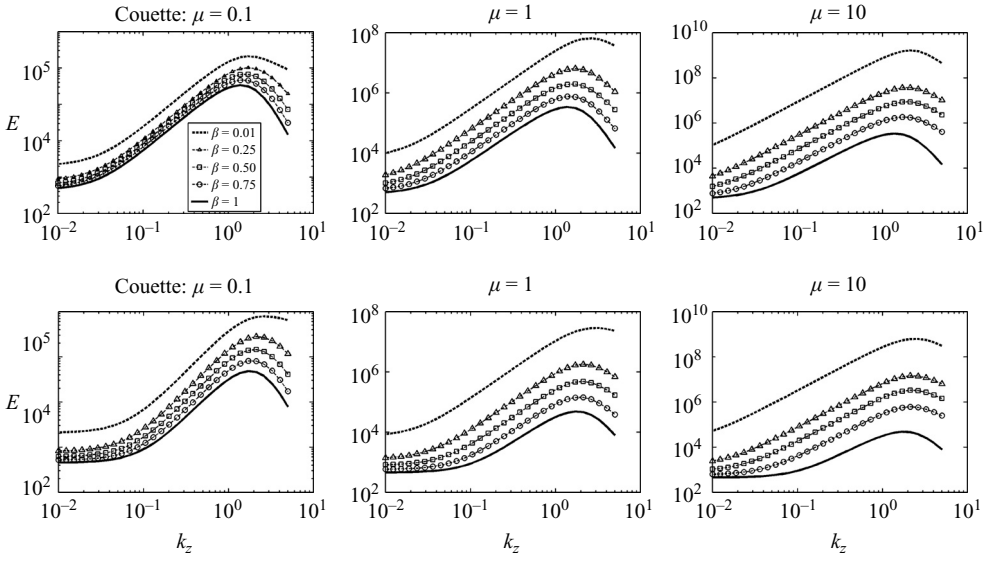

FIGURE 6. Variation of $E(k_z)$ for streamwise-constant perturbations at different values of β for $Re = 1000$ in both Couette and Poiseuille flows.

$1 - \beta$ in the operator $\boldsymbol{A}_{12}$ as β_3. Keeping β_2 and β_3 fixed, we found that increasing (decreasing) β_1 decreases (increases) the energy density for all non-zero k_z, suggesting that the viscous stress term suppresses disturbances. By analysing the effect of β_2 in a similar way, it is found that the vorticity diffusion term also suppresses disturbances. It should be noted that the energy density shows a similar dependence on the viscous stress and vorticity diffusion terms even at different μ and Re. The relative importance of these two terms was probed by comparing the variation in the energy density for a proportionate change in the prefactor of the viscous stress and the vorticity diffusion terms. For any elasticity number, the viscous stress term plays a dominant role in suppressing disturbances at higher Re, while at lower Re, the vorticity diffusion term is the dominant partner. The crossover occurs at $Re \approx 100$ for Poiseuille flow and $Re \approx 20$ for Couette flow.

The effect of β_3 on the energy density is more subtle. At smaller β_1 and β_2, a decrease (increase) in β_3 increases (decreases) the energy density for all k_z, suggesting that the polymeric stresses are suppressing the disturbances. At higher β_1 and β_2, the trend is reversed, and the values of β_1 and β_2 at which this reversal occurs depend upon μ and Re.

4.3. *Effect of* μ

Figure 7 shows the effect of the elasticity number on the energy amplification for $\beta = 0.1$ at several different Reynolds numbers. The general trends for other values of β and Re are similar. The increase in the energy amplification with μ is consistent with results of standard two-dimensional linear stability analyses for Poiseuille flow, which show that increasing the elasticity number initially lowers the critical Re at which instability occurs (Ho & Denn 1977; Sureshkumar & Beris 1995). However, whereas the linear stability analysis predicts stabilization beyond a critical value of the elasticity number, our analysis shows that energy amplification always increases with μ.

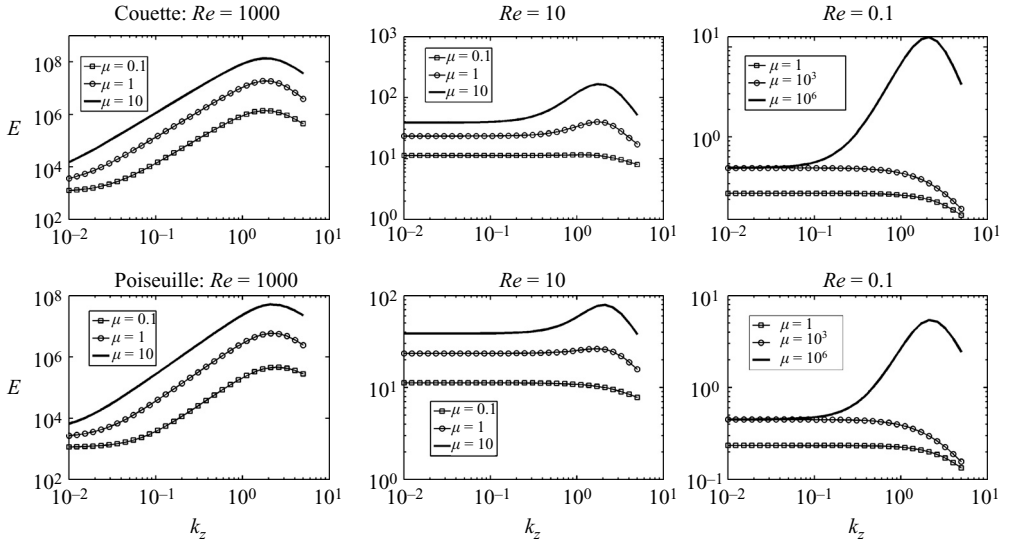

FIGURE 7. Variation of $E(k_z)$ at different values of μ for $k_x = 0$ and $\beta = 0.1$ in both Couette and Poiseuille flows.

The most striking feature of figure 7 is the observation that increasing μ beyond a certain value can cause the energy density to exhibit a maximum with respect to k_z. This is especially pronounced at low Reynolds numbers, where the energy density monotonically decreases for sufficiently small μ. This indicates that elasticity can produce considerable energy amplification in very viscous flows, with the most amplified disturbances having $O(1)$ spanwise wavenumber. Inspection of the terms in (2.2) shows that the elasticity number appears as a prefactor in front of the velocity gradient term, $(\nabla \boldsymbol{v} + (\nabla \boldsymbol{v})^T)$, and the polymeric stress terms, $\boldsymbol{\tau}$. We looked at the importance of these contributions and found that at intermediate and small β, the velocity gradient term suppresses disturbances, while the polymeric stress terms showed a complicated dependence on μ, suggesting that both terms are important.

4.4. *Comparison: Couette versus Poiseuille flow*

Figure 8 compares the energy amplification in Couette and Poiseuille flows with $Re = 1000$ and $\mu = 10$. Couette flow always exhibits a higher energy density, and the relative difference is largest for $\beta = 1$ (Newtonian case). It is also found that the relative difference decreases with a decrease in Re and β as well as with an increase in μ. For Newtonian fluids, the difference in the energy density in the two cases is due to the vortex stretching term; in Couette flow, the vortex stretching term is independent of y, while for Poiseuille flow it depends linearly on y. However, owing to the strong coupling between the various terms that is present in the viscoelastic case, we were unable to clearly identify terms which could explain the difference in the energy density between the two cases.

5. Conclusions

We have considered the problem of energy amplification in channel flows of Oldroyd-B fluids. By focusing on disturbances that enter the linearized governing equations in the form of body forces that are harmonic in the streamwise and

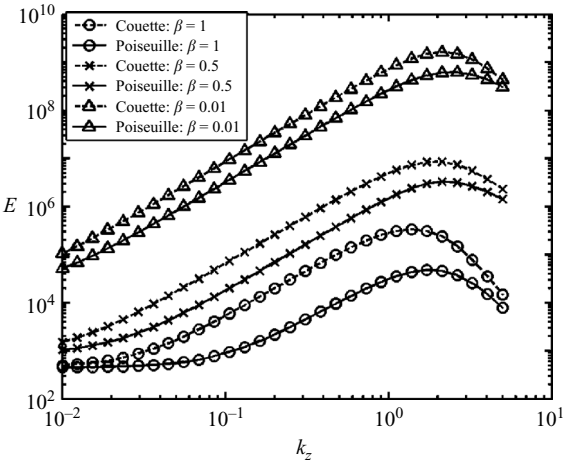

FIGURE 8. Comparison of the energy density in Couette and Poiseuille flows at different values of β for $Re = 1000$, $\mu = 10$.

spanwise directions and stochastic in the wall-normal direction and in time, we have been able to apply powerful tools from linear systems theory to characterize the behaviour of the ensemble-average energy density. Our results show that the presence of fluid elasticity can produce significant energy amplification relative to Newtonian fluids. This was observed both when varying the polymer-to-solvent viscosity ratio and the elasticity number. The most amplified disturbances tend to be elongated in the streamwise direction, and fluid elasticity tends to decrease the spanwise length scale. Determining the mechanism responsible for the energy amplification is challenging owing to the complex coupling of terms in the governing equations, and our results suggest that the interplay between viscous and elastic stresses plays a key role.

One of the most notable findings of this paper is the observation that elasticity can produce considerable energy amplification even when inertial effects are relatively weak. This energy amplification may then serve as a route through which channel flows of viscoelastic fluids become unstable. The large amplification could set up the initial conditions needed for transient growth, or could itself trigger nonlinear effects. Our results, which indicate that the most amplified disturbances are three-dimensional in nature, significantly augment prior work on viscoelastic channel flows, which has primarily focused on two-dimensional disturbances. The results also extend the work of Jovanović & Bamieh (2005) on Newtonian fluids to the viscoelastic case. We note that although we have considered disturbances in the form of body forces, the results raise the possibility that viscoelastic channel flows may be exceedingly sensitive to other types of disturbances. Future work on the stability of viscoelastic channel flows should thus consider the roles of external disturbances and three-dimensionality, as well as the mechanisms of energy amplification.

The work of N. H. and S. K. was partially supported by the Donors of The American Chemical Society Petroleum Research Fund. The work of M. R. J. was partially supported by the National Science foundation under CAREER Award CMMI-06-44793.

Appendix. Operators in the governing equations

The components of operator $\boldsymbol{A}$, defined in equation (2.3), are:

$$\boldsymbol{A}_{11} = \begin{bmatrix} (\beta/Re)\Delta^{-1}\Delta^2 - \mathrm{i}k_x\Delta^{-1}\overline{U}\Delta + \mathrm{i}k_x\Delta^{-1}\overline{U}'' & 0 \\ -\mathrm{i}k_z\overline{U}' & (\beta/Re)\Delta - \mathrm{i}k_x\overline{U} \end{bmatrix},$$

$$\boldsymbol{A}_{12} = \frac{1-\beta}{Re}\begin{bmatrix} \Delta^{-1} & 0 \\ 0 & I \end{bmatrix}\overline{\boldsymbol{A}}_{12},$$

$$\boldsymbol{A}_{21} = \frac{1}{k^2}\begin{bmatrix} a_{21}^{11} & a_{21}^{12} \\ a_{21}^{21} & a_{21}^{22} \\ a_{21}^{31} & a_{21}^{32} \\ a_{21}^{41} & a_{21}^{42} \\ a_{21}^{51} & a_{21}^{52} \\ a_{21}^{61} & a_{21}^{62} \end{bmatrix}, \qquad \boldsymbol{A}_{22} = \begin{bmatrix} D_i & 0 & 0 & 2\overline{U}' & 0 & 0 \\ 0 & D_i & 0 & 0 & 0 & 0 \\ 0 & 0 & D_i & 0 & 0 & 0 \\ 0 & \overline{U}' & 0 & D_i & 0 & 0 \\ 0 & 0 & 0 & 0 & D_i & \overline{U}' \\ 0 & 0 & 0 & 0 & 0 & D_i \end{bmatrix},$$

where $k^2 = k_x^2 + k_z^2$, $\mathrm{i} = \sqrt{-1}$, $\Delta = \partial_{yy} - k^2$ with Dirichlet boundary conditions, $\Delta^2 = \partial_{yyyy} - 2k^2\partial_{yy} + k^4$ with both Dirichlet and Neumann boundary conditions, $\overline{U}' = \mathrm{d}\overline{U}(y)/\mathrm{d}y$, and $\overline{U}'' = \mathrm{d}^2\overline{U}(y)/\mathrm{d}y^2$. The diagonal elements of $\boldsymbol{A}_{22}$, are given by $D_i = -\mathrm{i}k_x\overline{U} - 1/Wi$. Operator $\overline{\boldsymbol{A}}_{12}$ is defined as

$$\overline{\boldsymbol{A}}_{12} = \begin{bmatrix} k_x^2\partial_y & -k^2\partial_y & k_z^2\partial_y & -\mathrm{i}k_x(k^2+\partial_{yy}) & 2k_xk_z\partial_y & -\mathrm{i}k_z(k^2+\partial_{yy}) \\ -k_xk_z & 0 & k_xk_z & \mathrm{i}k_z\partial_y & k_x^2 - k_z^2 & -\mathrm{i}k_x\partial_y \end{bmatrix}.$$

The components of operator $\boldsymbol{A}_{21}$ are:

$$a_{21}^{11} = -2\left(\frac{k_x^2}{Wi}\partial_y + k_x^2\overline{\tau}_{xx}\partial_y - \mathrm{i}k_x\overline{\tau}_{xy}\partial_{yy}\right) - k^2\overline{\tau}'_{xx},$$

$$a_{21}^{12} = 2\left(\frac{k_xk_z}{Wi} + k_xk_z\overline{\tau}_{xx} - \mathrm{i}k_z\overline{\tau}_{xy}\partial_y\right),$$

$$a_{21}^{21} = k^2\left(\frac{2}{Wi}\partial_y + 2\mathrm{i}k_x\overline{\tau}_{xy}\right), \quad a_{21}^{22} = 0,$$

$$a_{21}^{31} = -\frac{2k_z^2}{Wi}\partial_y, \quad a_{21}^{32} = -\frac{2k_xk_z}{Wi},$$

$$a_{21}^{41} = \frac{\mathrm{i}k_x}{Wi}\partial_{yy} - k_x^2\overline{\tau}_{xy}\partial_y + k^2\left(\frac{\mathrm{i}k_x}{Wi} + \mathrm{i}k_x\overline{\tau}_{xx} + \overline{\tau}_{xy}\partial_y\right) - k^2\overline{\tau}'_{xy},$$

$$a_{21}^{42} = -\frac{\mathrm{i}k_z}{Wi}\partial_y + k_xk_z\overline{\tau}_{xy},$$

$$a_{21}^{51} = -\frac{2k_xk_z}{Wi}\partial_y - k_xk_z\overline{\tau}_{xx}\partial_y + \mathrm{i}k_z\overline{\tau}_{xy}\partial_{yy}, \quad a_{21}^{52} = \frac{k_z^2 - k_x^2}{Wi} - k_x^2\overline{\tau}_{xx} + \mathrm{i}k_x\overline{\tau}_{xy}\partial_y,$$

$$a_{21}^{61} = \frac{\mathrm{i}k_z}{Wi}(k^2 + \partial_{yy}) - k_xk_z\overline{\tau}_{xy}\partial_y, \quad a_{21}^{62} = \frac{\mathrm{i}k_x}{Wi}\partial_y - k_x^2\overline{\tau}_{xy},$$

where $\overline{\tau}'_{xx} = \mathrm{d}\overline{\tau}_{xx}(y)/\mathrm{d}y$.

Operators $\boldsymbol{B}$ and $\boldsymbol{C}$ are given by

$$\boldsymbol{B} = \begin{bmatrix} -\mathrm{i}k_x\Delta^{-1}\partial_y & -k^2\Delta^{-1} & -\mathrm{i}k_z\Delta^{-1}\partial_y \\ \mathrm{i}k_z & 0 & -\mathrm{i}k_x \end{bmatrix}, \quad \boldsymbol{C} = \frac{1}{k^2}\begin{bmatrix} \mathrm{i}k_x\partial_y & -\mathrm{i}k_z \\ k^2 & 0 \\ \mathrm{i}k_z\partial_y & \mathrm{i}k_x \end{bmatrix},$$

where Δ^{-1} is the inverse of the Laplacian operator.

The adjoints of operators $\boldsymbol{A}_{11}$, $\boldsymbol{A}_{12}$, $\boldsymbol{A}_{21}$, and $\boldsymbol{A}_{22}$ are determined using the following relations:

$$\begin{aligned} \langle \boldsymbol{\psi}_1, \boldsymbol{A}_{11}\boldsymbol{\psi}_1\rangle_e &= \langle \boldsymbol{A}_{11}^*\boldsymbol{\psi}_1, \boldsymbol{\psi}_1\rangle_e, \\ \langle \boldsymbol{\psi}_1, \boldsymbol{A}_{12}\boldsymbol{\psi}_2\rangle_e &= \langle \boldsymbol{A}_{12}^*\boldsymbol{\psi}_1, \boldsymbol{\psi}_2\rangle_2, \\ \langle \boldsymbol{\psi}_2, \boldsymbol{A}_{21}\boldsymbol{\psi}_1\rangle_2 &= \langle \boldsymbol{A}_{21}^*\boldsymbol{\psi}_2, \boldsymbol{\psi}_1\rangle_e, \\ \langle \boldsymbol{\psi}_2, \boldsymbol{A}_{22}\boldsymbol{\psi}_2\rangle_2 &= \langle \boldsymbol{A}_{22}^*\boldsymbol{\psi}_2, \boldsymbol{\psi}_2\rangle_2, \end{aligned}$$

where the inner product $\langle\cdot,\cdot\rangle_e$ determines the kinetic energy density of a harmonic perturbation and is related to the standard L_2 norm through (Butler & Farrell 1992)

$$\langle \boldsymbol{\psi}_1, \boldsymbol{\psi}_1\rangle_e = \langle \boldsymbol{\psi}_1, \boldsymbol{Q}\boldsymbol{\psi}_1\rangle_2,$$

where $\boldsymbol{Q}$ is a block diagonal linear operator given by

$$\boldsymbol{Q} = \frac{1}{k^2}\begin{bmatrix} -\Delta & 0 \\ 0 & \boldsymbol{I} \end{bmatrix}.$$

The adjoints of the components of $\boldsymbol{A}$ are determined using the above expression and are

$$\boldsymbol{A}_{11}^* = \begin{bmatrix} (\beta/Re)\Delta^{-1}\Delta^2 + \mathrm{i}k_x\Delta^{-1}\overline{U}\Delta + 2\mathrm{i}k_x\Delta^{-1}\overline{U}'\partial_y & -\mathrm{i}k_z\Delta^{-1}\overline{U}' \\ 0 & (\beta/Re)\Delta + \mathrm{i}k_x\overline{U} \end{bmatrix},$$

$$\boldsymbol{A}_{12}^* = \frac{1-\beta}{Re}\frac{1}{k^2}\overline{\boldsymbol{A}}_{12}^*,$$

$$\boldsymbol{A}_{21}^* = \begin{bmatrix} a_{21}^{*11} & a_{21}^{*12} & a_{21}^{*13} & a_{21}^{*14} & a_{21}^{*15} & a_{21}^{*16} \\ a_{21}^{*21} & a_{21}^{*22} & a_{21}^{*23} & a_{21}^{*24} & a_{21}^{*25} & a_{21}^{*26} \end{bmatrix},$$

$$\boldsymbol{A}_{22}^* = \begin{bmatrix} D_i^* & 0 & 0 & 0 & 0 & 0 \\ 0 & D_i^* & 0 & \overline{U}' & 0 & 0 \\ 0 & 0 & D_i^* & 0 & 0 & 0 \\ 2\overline{U}' & 0 & 0 & D_i^* & 0 & 0 \\ 0 & 0 & 0 & 0 & D_i^* & 0 \\ 0 & 0 & 0 & 0 & \overline{U}' & D_i^* \end{bmatrix},$$

where $D_i^* = \mathrm{i}k_x\overline{U} - 1/Wi$ and the operator $\overline{\boldsymbol{A}}_{12}^*$ is

$$\overline{\boldsymbol{A}}_{12}^* = \begin{bmatrix} k_x^2\partial_y & -k_xk_z \\ -k^2\partial_y & 0 \\ k_z^2\partial_y & k_xk_z \\ -\mathrm{i}k_x(k^2+\partial_{yy}) & \mathrm{i}k_z\partial_y \\ 2k_xk_z\partial_y & k_x^2-k_z^2 \\ -\mathrm{i}k_z(k^2+\partial_{yy}) & -\mathrm{i}k_x\partial_y \end{bmatrix}.$$

The components of the operator $\boldsymbol{A}_{21}^*$ are:

$$a_{21}^{*11} = -2\Delta^{-1}\left(\frac{k_x^2}{Wi}\partial_y + k_x^2(\overline{\tau}_{xx}\partial_y + \overline{\tau}'_{xx}) - \mathrm{i}k_x(\overline{\tau}_{xy}\partial_{yy} + \overline{\tau}''_{xy} + 2\overline{\tau}'_{xy}\partial_y)\right) + k^2\Delta^{-1}\overline{\tau}'_{xx},$$

$$a_{21}^{*12} = \Delta^{-1}k^2\left(\frac{2}{Wi}\partial_y + 2\mathrm{i}k_x\overline{\tau}_{xy}\right),$$

$$a_{21}^{*13} = -\Delta^{-1}\frac{2k_z^2}{Wi}\partial_y,$$

$$a_{21}^{*14} = \Delta^{-1}\left(\frac{\mathrm{i}k_x}{Wi}\partial_{yy} - k_x^2(\overline{\tau}_{xy}\partial_y + \overline{\tau}'_{xy}) + k^2\left(\frac{\mathrm{i}k_x}{Wi} + ik_x\overline{\tau}_{xx} + \overline{\tau}_{xy}\partial_y + \overline{\tau}'_{xy}\right)\right) + k^2\Delta^{-1}\overline{\tau}'_{xy},$$

$$a_{21}^{*15} = -\Delta^{-1}\left(\frac{2k_xk_z}{Wi}\partial_y + k_xk_z(\overline{\tau}_{xx}\partial_y + \overline{\tau}'_{xx}) - \mathrm{i}k_z(\overline{\tau}_{xy}\partial_{yy} + \overline{\tau}''_{xy} + 2\overline{\tau}'_{xy}\partial_y)\right),$$

$$a_{21}^{*16} = \Delta^{-1}\left(\frac{\mathrm{i}k_z}{Wi}(k^2+\partial_{yy}) - k_xk_z(\overline{\tau}_{xy}\partial_y + \overline{\tau}'_{xy})\right),$$

$$a_{21}^{*21} = 2\left(\frac{k_xk_z}{Wi} + k_xk_z\overline{\tau}_{xx} - \mathrm{i}k_z(\overline{\tau}_{xy}\partial_y + \overline{\tau}'_{xy})\right),$$

$$a_{21}^{*22} = 0, \quad a_{21}^{*23} = -\frac{2k_xk_z}{Wi}, \quad a_{21}^{*24} = -\frac{\mathrm{i}k_z}{Wi}\partial_y + k_xk_z\overline{\tau}_{xy},$$

$$a_{21}^{*25} = \frac{k_z^2-k_x^2}{Wi} - k_x^2\overline{\tau}_{xx} + \mathrm{i}k_x(\overline{\tau}_{xy}\partial_y + \overline{\tau}'_{xy}), \quad a_{21}^{*26} = \frac{\mathrm{i}k_x}{Wi}\partial_y - k_x^2\overline{\tau}_{xy}.$$

This operator simplifies in the case of Couette flow, as the base-state stresses ($\overline{\tau}_{xx}$ and $\overline{\tau}_{xy}$) are independent of y. Also, since the base-state velocity is a linear function of y, its first derivative is a constant and the second derivative is zero. The adjoints of operators $\boldsymbol{B}$ and $\boldsymbol{C}$ are determined from

$$\langle\boldsymbol{\psi}_1, \boldsymbol{B}\boldsymbol{d}\rangle_e = \langle\boldsymbol{B}^*\boldsymbol{\psi}_1, \boldsymbol{d}\rangle_2, \quad \langle\boldsymbol{v}, \boldsymbol{C}\boldsymbol{\psi}_1\rangle_2 = \langle\boldsymbol{C}^*\boldsymbol{v}, \boldsymbol{\psi}_1\rangle_e,$$

which yields

$$\boldsymbol{B}^* = \frac{1}{k^2}\begin{bmatrix} \mathrm{i}k_x\partial_y & -\mathrm{i}k_z \\ k^2 & 0 \\ \mathrm{i}k_z\partial_y & \mathrm{i}k_x \end{bmatrix}, \quad \boldsymbol{C}^* = \begin{bmatrix} -\mathrm{i}k_x\Delta^{-1}\partial_y & -k^2\Delta^{-1} & -\mathrm{i}k_z\Delta^{-1}\partial_y \\ \mathrm{i}k_z & 0 & -\mathrm{i}k_x \end{bmatrix}.$$

Based on this, it follows that $\boldsymbol{B}\boldsymbol{B}^* = \boldsymbol{I}$ and $\boldsymbol{C}^*\boldsymbol{C} = \boldsymbol{I}$, which is important for the energy density computations.

REFERENCES

Atalik, K. & Keunings, R. 2002 Non-linear temporal stability analysis of viscoelastic plane channel flows using a fully spectral method. *J. Non-Newtonian Fluid Mech.* **102**, 299–319.

Bamieh, B. & Dahleh, M. 2001 Energy amplification in channel flows with stochastic excitations. *Phys. Fluids* **13**, 3258–3269.

Bird, R. B., Curtiss, C. F., Armstrong, R. C. & Hassager, O. 1987 *Dynamics of Polymeric Liquids*, vol. 2. Wiley.

Boyd, J. 1989 *Chebyshev and Fourier Spectral Methods*. Springer.

Butler, K. M. & Farrell, B. F. 1992 Three-dimensional optimal perturbations in viscous shear flow. *Phys. Fluids* A **4**, 1637–1650.

Canuto, C., Hussaini, M. Y., Quarteroni, A. & Zang, T. A. 1988 *Spectral Methods in Fluid Dynamics*. Springer.

Curtain, R. F. & Zwart, H. J. 1995 *An Introduction to Infinite-Dimensional Linear System Theory*. Springer.

Doering, C., Eckhardt, B. & Schumacher, J. 2006 Failure of energy stability in Oldroyd-B fluids at arbitrarily low Reynolds numbers. *J. Non-Newtonian Fluid Mech.* **135**, 92–96.

Farrell, B. F. & Ioannou, P. J. 1993 Stochastic forcing of the linearized Navier-Stokes equations. *Phys. Fluids* A **5**, 2600–2609.

Gorodtsov, V. & Leonov, A. 1967 On a linear instability of plane parallel Couette flow of viscoelastic fluids. *J. Appl. Math. Mech. (Prikl. Mat. Mech.)* **31**, 310–319.

Grossmann, S. 2000 The onset of shear flow turbulence. *Rev. Mod. Phys.* **72**, 603–618.

Ho, T. C. & Denn, M. M. 1977 Stability of plane Poiseuille flow of a highly elastic liquid. *J. Non-Newtonian Fluid Mech.* **3**, 179–195.

Hoda, N., Jovanović, M. R. & Kumar, S. 2008 Frequency responses of the 2D/3C model in channel flows of Oldroyd-B fluids. *J. Fluid Mech*. (to be submitted).

Jovanović, M. R. & Bamieh, B. 2005 Componentwise energy amplification in channel flows. *J. Fluid Mech.* **534**, 145–183.

Kumar, A. S. & Shankar, V. 2005 Instability of high-frequency modes in viscoelastic plane Couette flow past a deformable wall at low and finite Reynolds number. *J. Non-Newtonian Fluid Mech.* **125**, 121–141.

Kupferman, R. 2005 On the linear stability of plane Couette flow for an Oldroyd-B fluid and its numerical approximation. *J. Non-Newtonian Fluid Mech.* **127**, 169–190.

Landahl, M. T. 1975 Wave breakdown and turbulence. *SIAM J. Appl. Maths* **28**, 735–756.

Larson, R. G. 1999 *The Structure and Rheology of Complex Fluids*. Oxford University Press.

McComb, W. D. 1991 *The Physics of Fluid Turbulence*. Oxford University Press.

Meulenbroek, B., Storm, C., Morozov, A. N. & Saarloos, W. 2004 Weakly nonlinear subcritical instability of visco-elastic Poiseuille flow. *J. Non-Newtonian Fluid Mech.* **116**, 235–268.

Morozov, A. N. & Saarloos, W. 2005 Subcritical finite-amplitude solutions for plane Couette flow of viscoelastic fluids. *Phys. Rev. Lett.* **95**, 024501-1-024501-4.

Orszag, S. A. 1971 Accurate solution of the Orr-Sommerfeld equation. *J. Fluid Mech.* **50**, 689–703.

Renardy, M. & Renardy, Y. 1986 Linear stability of plane Couette flow of an upper convected Maxwell fluid. *J. Non-Newtonian Fluid Mech.* **22**, 23–33.

Romanov, V. A. 1973 Stability of plane-parallel Couette flow. *Funct. Anal. Applics.* **7**, 137–146.

Schmid, P. J. 2007 Nonmodal stability theory. *Annu. Rev. Fluid Mech.* **39**, 129–162.

Schmid, P. J. & Henningson, D. S. 2001 *Stability and Transition in Shear Flows*. Springer.

Sureshkumar, R. & Beris, A. N. 1995 Linear stability analysis of viscoelastic Poiseuille flow using a Arnoldi-based orthogonalization algorithm. *J. Non-Newtonian Fluid Mech.* **56**, 151–182.

Sureshkumar, R., Smith, M. D., Armstrong, R. C. & Brown, R. A. 1999 Linear stability and dynamics of viscoelastic flows using time-dependent numerical simulations. *J. Non-Newtonian Fluid Mech.* **82**, 57–104.

Trefethen, L. N., Trefethen, A. E., Reddy, S. C. & Driscoli, T. A. 1993 Hydrodynamic stability without eigenvalues. *Science* **261**, 578–584.

Weideman, J. A. C. & Reddy, S. C. 2000 A MATLAB differentiation matrix suite. *ACM T. Math. Software* **26**, 465–519.

Wilson, H. J., Renardy, M. & Renardy, Y. 1999 Structure of the spectrum in zero Reynolds number shear flow of the UCM and Oldroyd-B liquids. *J. Non-Newtonian Fluid Mech.* **80**, 251–268.

Zhou, K., Doyle, J. C. & Glover, K. 1996 *Robust and Optimal Control*. Prentice Hall.